Evidence of Mixed-Ligand Complexes in Cu−CHA by Reaction of Cu Nitrates with NO/NH3 at Low Temperature

UNIVERSITÀ DEGLI STUDI DI TORINO

Evidence of mixed-ligand complexes in Cu-CHA by reaction of Cu nitrates with NO/NH_3 at low temperature

Chiara Negri [a], Elisa Borfecchia [a], Michele Cutini [a], Kirill A. Lomachenko [b], Ton V.W. Janssens [c], Gloria Berlier [a]* and Silvia Bordiga [a]

[1] Dr. Chiara Negri, Dr. Elisa Borfecchia, Dr. Michele Cutini, Prof. Gloria Berlier * and Prof. Silvia Bordiga, Department of Chemistry, NIS Centre and INSTM Reference Center, University of Turin, Via Giuria 7, Turin, 10125 Italy. e-mail: gloria.berlier@unito.it
[b] Dr. Kirill A. Lomachenko, European Synchrotron Radiation Facility, 71 Avenue des Martyrs, CS 40220, Grenoble Cedex 9, 38043 France.
[c] Dr. Ton V.W. Janssens, Umicore Denmark ApS, Nøjsomhedsvej 20, Kgs. Lyngby, 2800 Denmark

Table of contents:

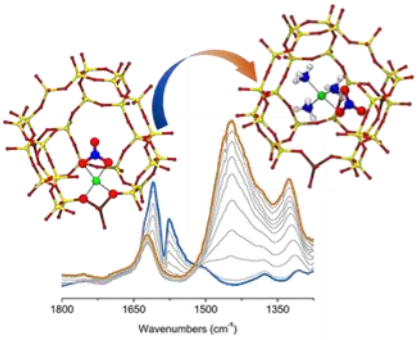

The detachment of framework-interacting Cu-nitrates in Cu-CHA in a NO/NH_3 flow is followed at 50 °C by *in situ* FTIR, Diffuse Reflectance UV-Vis and XAS spectroscopies, showing the formation of mixed-ligand mobile $[Cu^{II}(NH_3)_3(NO_3)]^+$ complexes.

Abstract:

The reactivity with a NO/NH_3 mixture of Cu-nitrate complexes formed on the surface of a Cu-CHA catalyst active in the Selective Catalytic Reduction of NO_x with NH_3 (NH_3-SCR) was followed at 50 °C by *in situ* spectroscopic techniques. The catalyst (Si/Al=15; Cu/Al=0.5) was first exposed to NO/O_2 (mimicking the SCR oxidative half-cycle), mainly resulting in the formation of chelating bidentate framework-interacting Cu^{II}-nitrates. These intermediates were gradually detached from the framework in the presence of NO/NH_3 (or NH_3 alone), forming mixed-ligand mobile $[Cu^{II}(NH_3)_3(NO_3)]^+$ complexes, with infrared bands at 1624 (δNH_3), 1430 and 1325 cm^{-1} (monodentate nitrate νNO_{2asym} and νNO_{2sym}, respectively). X-ray absorption and Diffuse Reflectance UV-Vis spectroscopies showed that during this transformation the Cu^{II}/Cu^{I} reduction, observed under similar conditions at 200 °C, hardly occurred. DFT calculations confirmed the stability of nitrate ligands in the monodentate conformation in $[Cu^{II}(NH_3)_3(NO_3)]^+$ complexes when solvated by ammonia. The resulting structure was successfully used to fit the corresponding experimental EXAFS spectra. The gradual change of ligands in the Cu^{II} coordination sphere was confirmed by the blue shifts of both $d-d$ and Ligand to Metal Charge Transfer bands in Diffuse Reflectance UV-Vis spectra, with formation of features (27500, 32000 and 38000 cm^{-1}) ascribable to the mixed-ligand configuration.

Introduction

The Selective Catalytic Reduction with ammonia (NH_3-SCR) reaction is at the basis of one of the most important technologies for the abatement of NO_x emissions from diesel engines. An important breakthrough concerning the catalyst came from the discovery of Cu-exchanged chabazite (Cu-CHA) performance, superior to any other previously studied metal-exchanged zeolite. Small pore Cu-CHA is thus the catalyst of choice for diesel engines SCR, thanks to its excellent performance and hydrothermal stability over a wide range of temperatures.[1] Moreover, the structural simplicity of chabazite, allowing for very sophisticated experimental and computational studies, makes it a model system to solve fundamental issues of structure-activity correlations in the wider context of transition metal-exchanged zeolites.[2]

The state of the Cu ions in Cu-CHA depends on the Al distribution, on the Si/Al and Cu/Al ratios and on the presence of an oxidizing or reducing atmosphere. In an oxidizing atmosphere, Cu^{II} ions can be stabilized in correspondence of a single Al framework atom, resulting in a $Z[Cu^{II}(OH)]$, or form a Z_2Cu^{II} site (being Z the framework negative charge induced by the presence of Al).[3] Both species can be reversibly transformed into $Z\text{-}Cu^{I}$ by changing the gas atmosphere. This redox behavior is at the basis of the SCR reactivity. Indeed, both the *standard* (r1) and the *fast* (r2) SCR reactions can be divided in two distinct half-cycles: Cu^{II} reduction (with release of N_2 and H_2O) and Cu^{I} re-oxidation, necessary to re-establish the active site for NO_x decomposition.[4]

$$4NH_3 + 4NO + O_2 \rightarrow 4N_2 + 6H_2O \qquad \text{(r1)}$$

$$2NH_3 + NO_2 + NO \rightarrow 2N_2 + 3H_2O \qquad \text{(r2)}$$

The activation of molecular O_2 over Cu^{I} is a key step in the NH_3-SCR reaction (Eq. r1), and a number of possible pathways for this part of the reaction have been discussed.[5] As molecular O_2 does not interact with Cu^{II}, this activation must imply a reaction with a Cu^{I} species. Isolated framework-interacting Cu^{I} sites are able to activate O_2 and to form Cu^{II} only at high temperature.[4, 6] Therefore, such an O_2 activation pathway is not viable for NH_3-SCR at low temperatures. Paolucci *et al*.[5c] and Gao *et al*.[7] have recently pinpointed that mobile NH_3-solvated $[Cu^{I}(NH_3)_2]^+$ complexes facilitate the formation of Cu-pairs, which make O_2 activation at 200 °C feasible. Furthermore, O_2 activation is easier in the presence of NO, resulting in the formation of nitrites and nitrates on the surface of the catalyst, in the absence of NH_3.[5a, 8]

In the reduction half-cycle, a complete reduction of Cu^{II} to Cu^{I} is observed at 200 °C in the presence of NO/NH_3. This results in the formation of the mobile $[Cu^{I}(NH_3)_2]^+$ complexes proposed to be active for O_2 activation at low temperature.[4, 6, 9] NH_3 alone is a less efficient reducing agent, producing a mixture of $[Cu^{I}(NH_3)_2]^+$, $[Cu^{II}(NH_3)_4]^{2+}$ and/or $[Cu^{II}(NH_3)_3(OH)]^+$ complexes. [3c, 4, 9c] Many studies on both half-cycles thus point to the importance of ligand-stabilized Cu species in Cu-CHA catalysts for NH_3-SCR.

The role of the nitrate/nitrite species formed in the presence of NO/O_2 in the SCR mechanism is still not well understood.[4-5, 8, 10] In particular, the equilibrium between Cu-nitrate and Cu-nitrite, and their reactivity with NO and NH_3 to release N_2 and H_2O have been studied. It was proposed that both species can react with adsorbed NH_3, giving NH_4NO_3 or NH_4NO_2.[11] Ammonium nitrite is expected to easily decompose to

N_2 and H_2O.[12] On the other hand NH_4NO_3, stable up to 170 °C, could deactivate the catalyst by pore blocking and give a side reaction leading to undesired N_2O at slightly higher temperatures.[11b, 12b, 13] Nonetheless, NH_4NO_3 deposited on the catalyst surface can react with NO, producing NO_2 which is required for the *fast* SCR.[12b, 13a-c, 14, 15, 16] Furthermore, NO can directly reduce NH_4NO_3 to NH_4NO_2 which, as previously mentioned, easily decomposes to N_2 and H_2O already at 100 °C.[12b, 13d, 14] However, both *standard* and *fast* reactions can be explaining without the role of NH_4NO_3. [4, 8, 17]

To improve our understanding of the NH_3-SCR reaction over Cu-CHA catalysts, information about the Cu-species formed under NH_3-SCR conditions is needed, in particular at low temperature, which is crucial for the performance in the cold start of diesel engines. In this article, we present an *in situ* FTIR study about the reactivity of Cu^{II}-(N,O) species, formed by reaction of Cu-CHA with NO/O_2 (oxidative half-cycle), with the NO/NH_3 mixture (reduction half-cycle). Measurements are carried out at 50 °C, the lowest temperature attainable without serious water contamination of the catalyst, to get information on the low temperature stability and reactivity of the formed complexes. X-ray absorption spectroscopy and UV-Vis-NIR diffuse reflectance spectroscopies are used as complementary techniques to follow the oxidation state and the coordination environment of Cu during the reactions, with the support of DFT calculations to assess the stability of the proposed ligand-stabilized Cu-complexes, which could play a role in the low-temperature SCR reaction.

Experimental

In situ spectroscopies

FTIR spectra were recorded in transmission mode on a PerkinElmer System 2000 infrared spectrophotometer, equipped with a MCT detector; 128 interferograms (recorded at 2 cm^{-1} resolution) were typically averaged for each spectrum. Zeolite powder was pressed into a self-supporting pellet of ca. 15 mg and placed inside a commercial FTIR reactor cell (AABSPEC, no. 2000-A multimode), able to work in controlled gas atmosphere and temperature. The spectra reported in this work (excluding the right-hand panel of Figure 1) were background subtracted using as a reference the spectrum of the activated zeolite before gas admission. NH_4NO_3 was measured in transmission mode after dilution in KBr.

UV-Vis-NIR spectra were recorded in the 2500-200 nm range (50000 – 4000 cm^{-1}) at 1 nm resolution on a Varian Cary 5000 spectrophotometer, equipped with a R928 PMT UV-Vis detector and a cooled PbS photocell NIR detector. Spectra were collected with a Praying Mantis® element, coupled with a low temperature (LT) reaction chamber. Measurements were carried out on sieved samples (300 and 150 μm), pelletized with a hydraulic press and successively crushed and sieved. Teflon powder in the same LT cell was measured as a reference. Spectra are reported as relative reflectance (R%), defined as:

$$R_{\%} = R_{sample}/R_{reference} \cdot 100$$

$[Cu^{II}(NH_3)_4]^{2+}$ in aqueous solution was measured in transmission mode in the same instrument.

X-ray Absorption Spectroscopy (XAS) data were collected at the BM23 beamline[18] of the European Synchrotron Radiation Facility (ESRF, Grenoble, France) using the Microtomo reactor cell.[19] The Cu-CHA catalyst was prepared in the form of a self-supporting pellet (~ 100 mg/1.3 cm^2, resulting in an edge jump $\Delta\mu x = 0.6$ for a total absorption after the edge of $\mu x = 2.5$). Cu K-edge XAS measurements were performed in transmission mode, employing a double-crystal Si(111) monochromator for the incident energy scan, a pair of flat Si mirrors at 2.5 mrad angle for harmonics rejection, and ionization chambers to detect incident

(I_0) and transmitted ($I_{1,2}$) photons. A Cu metal foil was measured simultaneously using a third ionization chamber I_2, for energy calibration purposes.[20] XAS spectra of ~ 20 min each (energy range 8800 – 9965 eV; pre-edge region energy step = 5 eV, edge region energy step = 0.3 eV, constant k-space sampling Δk = 0.035 $Å^{-1}$ in the EXAFS region; acquisition time of 1 s/point in the whole energy range) were measured at stationary conditions. The three corresponding $\mu(E)$ curves were averaged after checking reproducibility among the consecutive acquisitions.

Experiment description

The gas flow used in the experiments was 50 ml/min (100 ml/min for XAS). In all the experiments, the measured catalyst was first treated in O_2 at 400 °C for 60 min (heating rate 5 °C/min), then cooled to 50 °C (cooling rate 3°C/min) in O_2 and treated with 10% O_2/1000 ppm NO in inert diluent. After reaching steady state conditions (typically 30/60/120 min for FTIR/UV-Vis/XAS, respectively) the system purged with N_2 was then exposed to a mixture of 1000 ppm NO and 1200 ppm NH_3. The measurement cells inlet lines were heated to 130 °C to minimize NH_3 adsorption in the equipment. All reported data were measured at 50 °C.

XAS data analysis

The Athena software (Demeter package) was used to align XAS data by using the corresponding Cu metal foil spectra and for normalization to unity of the edge jump.[21] The same program was used for the extraction of the $\chi(k)$ function. R-space FT-EXAFS spectra were obtained by calculating the Fourier transform of the $k^2\chi(k)$ functions in the (2.4 – 12.4) $Å^{-1}$ k-range. DFT-assisted EXAFS fits were performed in R-space, in the ΔR = 1.0 – 4.0 Å range, on the FT of the k^2-weigthed $\chi(k)$ EXAFS spectra transformed in the 2.4 – 12.4 $Å^{-1}$ range, resulting in 19 independent points ($2\Delta k\Delta R/\pi > 19$). Phases and amplitudes have been calculated by FEFF6 code,[22] using the Artemis software from the Demeter package.[21]

Phase and amplitude of each path were calculated using as starting guess the DFT-optimized geometries of $[Cu^{II}(NH_3)_3(NO_3)]^+$ and of $[Cu^{II}(NH_3)_4]^{2+}$. We included all the single scattering (SS) paths and the principal multiple scattering (MS) paths involving O and N atoms in the investigated R-space range. To limit the number of fitting variables, all the included paths were optimized with the same amplitude factor (S_0^2) and energy shift (ΔE). The SS and MS paths falling in the 2.5 – 4.0 Å range were included in the fitting model of the $[Cu^{II}(NH_3)_3(NO_3)]^+$ structure with an isotropic parametrization strategy. These paths were parametrized considering a global isotropic contraction/expansion factor α_{far} and a Debye-Waller (DW) factor σ^2_{far} increasing as the square root of the distance $R_{eff,i}$ of the i^{th} scattering atom from the absorber ($\Delta R_i = \alpha_{far}(R_{eff,i}/R_0)$; $\sigma^2_i = \sigma^2_{far}(R_{eff,i}/R_0)^{1/2}$, where R_0 refers to the shortest path of the group, resulting in only two optimized parameters: α_{far}, σ^2_{far}).

Computational Details

All calculations were performed within the DFT approach, using the Gaussian 09 program.[23] Simulations were run using the hybrid B3LYP functional,[24] corrected for dispersion by the D3 scheme.[25] We employed two basis sets (BSs) to run geometry optimizations, i.e. BS1 and BS2. In BS1 N, O, C and H atoms are described by a VTZP quality basis set.[26] For Cu we employed a TZV basis set,[27] plus a polarization p function with coefficient 0.155065 for Cu.[28] BS2 is the Def2-TZVP basis set as coded in the Gaussian 09 suit.[29] The difference between BS1 and BS2 is on the description of the Cu atom, which has no polarization function (f orbitals) in BS1. Some control simulations were run also with the much larger Def2-QZVP basis set.[29] Only slight differences were noticed between BS2 and Def2-QZVP results, confirming that a TZVP quality BS is enough for our purposes. Solvation effects were taken into account using the PCM polarized

continuum model.[30] Solvation by ammonia was modelled using the default PCM values, then changing the dielectric constant of the solvent to 14.01, corresponding to liquid ammonia.[31] $[Cu^{II}(NH_3)_3(NO_3)]^+$ complexes in solution and in gas phase have charge +1 and are spin polarized with ground state with doublet character. The $[Cu(NH_3)_4]^{2+}$ complex structure was relaxed in water solution using the B3LYP-D3/BS2 approach. We employed the default PCM parameters for simulating liquid water, as coded within the Gaussian 09 suit. The complex has charge of +2 and is spin polarized with a doublet character ground state.

Results and discussion

In situ FTIR: reactivity of Cu^{II}-(N,O) species with NO/NH_3

In a recent work, the low temperature reactivity of the NO/O_2 mixture on a series of Cu-CHA catalysts with different composition has been investigated by *in situ* FTIR spectroscopy.[10] On the Cu-CHA catalyst studied in this work (Si/Al=15; Cu/Al=0.5), NO/O_2 exposure at 50 °C results in the formation of $Z[Cu^{II}(NO_3)]$, *i.e.* chelating bidentate Cu^{II} nitrates coordinated to framework oxygens in the proximity of a charge balancing Al site, with a minor amount of framework-coordinated monodentate Cu^{II} nitrates and of the nitrosonium ion NO^+. This low-temperature reactivity can be explained by the presence of small amounts of NO_2 in the flow, formed by gas phase reaction of NO and O_2. In this work, the reactivity of these Cu^{II}-(N,O) species towards the NO/NH_3 mixture is studied.

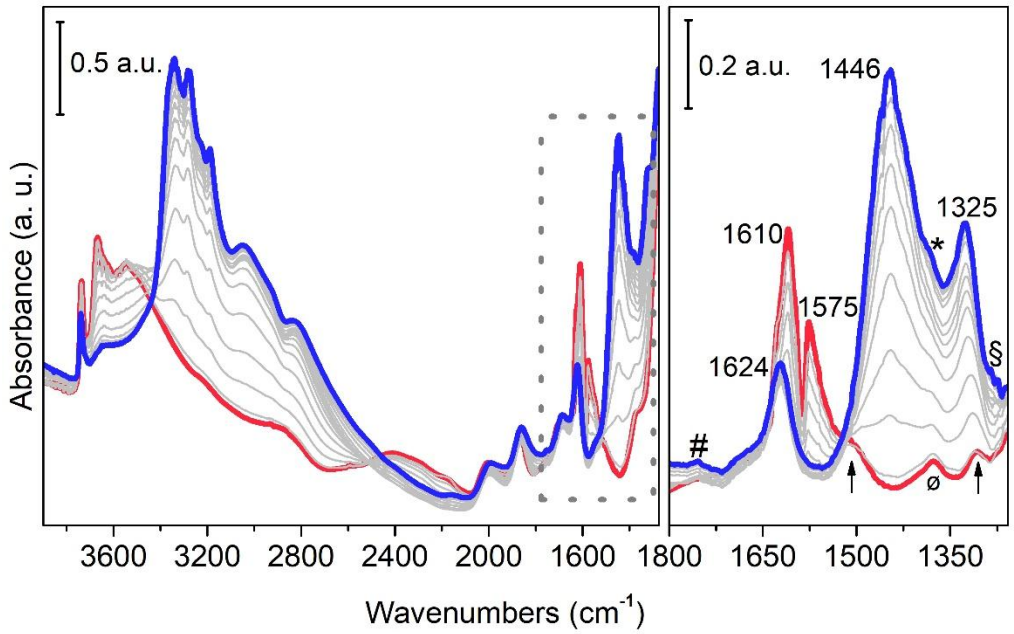

*Figure 1. In situ FTIR spectra of Cu-CHA during exposure to NO/NH_3 (thin grey and blue thick curves: intermediates and final state after 30 min) after equilibration in the NO/O_2 flow (red thick line). The relevant bands in the bending mode region are magnified in the right-hand panel after subtracting the zeolite reference spectrum. Symbols: #: NO_3^- $\nu_{sym}+\delta_{in\text{-}plane}$ combination mode; *: NO_3^- ν_{asym}; §: Cu-NH_3 out of plane wagging mode; ø: δH_3O^+; arrows: νNO_{2sym} and νNO_{2asym} modes* of Cu^{II} *monodentate nitrates*

Figure 1 reports the development of the FTIR spectra obtained when contacting the catalyst with the reactive gas feed. Before the exposure to 1000 ppm of NO and 1200 ppm of NH_3 at 50 °C, the Cu-CHA surface has been saturated with nitrates, formed by exposing the O_2-activated catalyst to 1000 ppm NO

and 10% O_2 at 50 °C.[10] The formation of adsorbed nitrates after this treatment is confirmed by the peaks related to chelating bidentate Cu^{II} structures (1610-1575 cm^{-1}) and monodentate ones (1500, 1310 cm^{-1}, indicated with arrows in Figure 1, right hand panel).[10, 17, 32] A small amount of NO^+, ascribed to the reaction of NO/O_2 with residual Brønsted sites is also observed (2159 cm^{-1}), resulting in the formation of small amounts of water (H_3O^+ signals at 1380 cm^{-1} labelled with ø, see Negri *et al*. for more details[10]).

When the catalyst is exposed to the NO/NH_3 mixture, changes are observable in the entire spectral region. In the OH stretching region (νOH), the growth of a complex series of bands between 3500 and 3000 cm^{-1} is evident, in parallel with the consumption of the νOH mode of Brønsted groups (3582 and 3665 cm^{-1}). In the low frequency region (1800-1250 cm^{-1}, magnified in right-hand panel of Figure 1), a clear transformation of the chelating bidentate Cu^{II} nitrates (bands at 1610 and 1575 cm^{-1}) into new species with intense bands at 1446 and 1325 cm^{-1} is clearly evidenced by the isosbestic point at 1518 cm^{-1}. Other features are the band at 1624 cm^{-1} and a weak peak at 1755 cm^{-1} (labelled with #).

The broad absorption between 3500 and 3000 cm^{-1} is due to the NH stretching modes (νNH) of adsorbed NH_3 molecules and NH_4^+ ions formed upon protonation by residual Brønsted sites.[9a, 33] The bands at 1624 and 1446 cm^{-1} have been already reported in literature for Cu-CHA materials [4, 9a, 11b] and were assigned to the bending modes of ammonia adsorbed on Cu ions (δNH_3) and of ammonium ions (δNH_4^+). A band similar to the 1325 cm^{-1} one (1297 cm^{-1}) is reported by Janssens *et al.*,[4] where NO/NH_3 were dosed on the sample after nitrate formation at 200 °C, and it has been assigned to the symmetric δNH_3 mode of ammonia in $[Cu^I(NH_3)_2]^+$ complexes. The assignment was supported by DFT calculations, predicting frequencies at 1640 and 1321 cm^{-1} for the δ_{asym} and δ_{sym} modes, respectively. This assignment is re-discussed in the following.

The reactivity of pre-adsorbed nitrates was also followed in the presence of NH_3 or NO alone, to study the role of each reactant in the NO/NH_3 mixture. NO showed the same effect already observed at 200 °C, that is a gradual decrease of the adsorbed nitrate complexes, which was explained with a displacement in the nitrate/nitrite equilibrium (not reported).[17] The reactivity of nitrates with NH_3 is reported in Figure 2 (right-hand panel), where it is directly compared to the spectra obtained while dosing NH_3 alone on the fresh O_2-activated catalyst (left-hand panel).

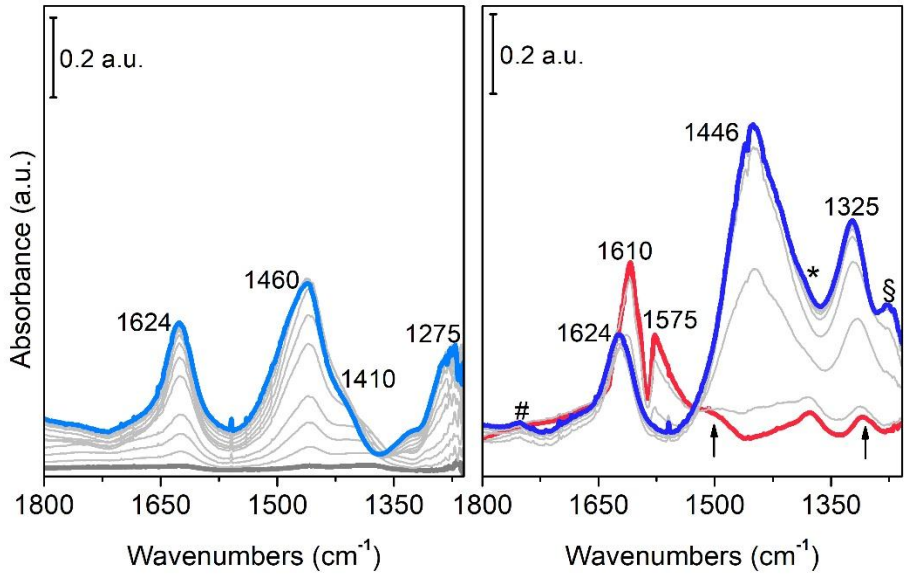

*Figure 2. In situ FTIR spectra of Cu-CHA during exposure to NH_3: (left) on the fresh O_2-activated catalyst and (right) after equilibration in NO/O_2. Left: thick grey and light blue curves measured after 2 and 30 min in NH_3; right: red thick line after equilibration in NO/O_2; blue thick line after 30 minutes in NH_3. Grey thin lines: intermediates spectra. Symbols: #: NO_3^- $\nu_{sym}+\delta_{in\text{-}plane}$ combination mode; *: NO_3^- ν_{asym}; §: Cu-NH_3 out of plane wagging mode; arrows: νNO_{2sym} and νNO_{2asym} modes* of Cu^{II} *monodentate nitrates.*

Clearly, the presence of pre-adsorbed nitrates on the surface of the catalyst affect the final state after 30 minutes in NH_3 (compare light blue and blue curves in the two panels of Figure 2). The bands in the left-hand panel spectra, obtained upon NH_3 exposure on the O_2-activated catalyst, are similar to literature reports.[9a, 34] As previously mentioned, the peak at 1624 cm^{-1} is related to the bending mode of Cu-NH_3 complexes, with the corresponding out-of-plane wagging mode at 1275 cm^{-1} (labelled with § in Figure 1 and in the right-hand panel of Figure 2). Notice that NH_3 is a strong Lewis base, so that its position is not sensitive to the oxidation state of the involved Cu ions. In other words, it is not possible to discriminate by this technique between $[Cu^{I}(NH_3)_2]^+$ and $[Cu^{II}(NH_3)_4]^{2+}$/$[Cu^{II}(NH_3)_3(OH)]^+$ species. On the contrary, the peak at 1460 cm^{-1} related to δNH_4^+ has been shown by Giordanino *et al.* to be strongly influenced by the environment and measurement temperature.[9a] Indeed, below 400 °C, $NH_4^+ \cdot \bullet nNH_3$ solvated species ($n \geq 1$) gave a band centred at 1463 cm^{-1}, which was red-shifted at higher temperature for 'free' NH_4^+ ions (two overlapping components at 1450 and 1400 cm^{-1} due to δ_{asym} and δ_{sym}, respectively).

When NH_3 is dosed on the catalyst previously saturated with Cu nitrates, the final state closely resembles what obtained by dosing NO/NH_3 after the same pre-treatment (Figure 1), and cannot be simply explained by the presence of Cu-NH_3 complexes and NH_4^+ ions. In particular, the 1624 cm^{-1} band is very similar in the three experiments, in shape, position and intensity. On the contrary, the band assigned to NH_4^+ ions shifts from 1460 to 1446 cm^{-1} when NH_3 (or NO/NH_3) is dosed on pre-adsorbed nitrates, being significantly more intense. Moreover, the sharp peak at 1325 cm^{-1} is clearly not formed when dosing NH_3 on the catalyst without pre-adsorbed nitrates, implying the presence of extra ligands in the coordination sphere of the Cu ions.

These spectroscopic observations thus provide the following information on the low-temperature reactivity of Cu-CHA catalysts towards the SCR reactants: (i) as recently shown, chelating nitrates are formed at temperature as low as 50 °C;[10] (ii) chelating nitrates readily react with NH_3/NO (or NH_3 alone) at 50 °C; (iii) the resulting adsorbed species are similar irrespectively of the presence of NO in the flow, indicating the primary role of NH_3 in the reaction; (iv) the formed complexes cannot be simply interpreted in terms of $[Cu^{I}(NH_3)_2]^+$, $[Cu^{II}(NH_3)_4]^{2+}$ or $[Cu^{II}(NH_3)_3(OH)]^+$ complexes, implying the formation of a different ligand-stabilized species.

Interpretation of in situ FTIR results

The comparison reported in Figure 2 clearly shows that the bands at 1446 and 1325 cm^{-1} cannot be related to the formation of NH_3-solvated Cu^{II}/Cu^{I} ions. They depend on the pretreatment of the catalyst, more precisely on the reaction of NH_3 with pre-adsorbed Cu^{II}-(N,O) species. Similar bands have been reported on a TiO_2-supported vanadia catalyst by Kantcheva *et al.*,[13d] on a vanadium-based catalyst by Nova *et al.*[12a] and on copper chabazite by Ruggeri *et al.*[11b] Kantcheva *et al.*[13d] proposed that ammonium nitrite and ammonium nitrate are formed when NH_3 reacts with adsorbed nitrates, or by exposure of NO_2 to the vanadia-TiO_2 catalyst saturated with NH_3. To investigate this hypothesis, the final states obtained after dosing NH_3 on the O_2-activated samples and NO/NH_3 on the surface saturated with nitrates (blue curves in Figure 2, left panel, and Figure 1, respectively) are directly compared with the spectrum of NH_4NO_3 (Figure 3). For the sake of comparison, spectra were normalized to pellet thickness.

The infrared spectrum of NH_4NO_3 is given by the vibrations of the two involved ions: i) the stretching mode of free NO_3^- ions ($\nu_{asym}NO_3^-$) at 1380 cm^{-1} and ii) a broad band in the 3500-3000 cm^{-1} region, due to the ν_{asym} mode of NH_4^+ ions. [35] The δNH mode of NH_4^+ (δ_{asym}, between 1415 and 1435 cm^{-1}) in ammonium nitrate crystal phases[35a] is overlapped with the $\nu_{asym}NO_3^-$ one, while the weak signal at 1760 cm^{-1} is the combination mode of the $\nu_{sym}NO_3^-$ symmetric stretching (Raman active) and the NO_3^- in plane deformation ($\delta_{in\ plane}$) mode.

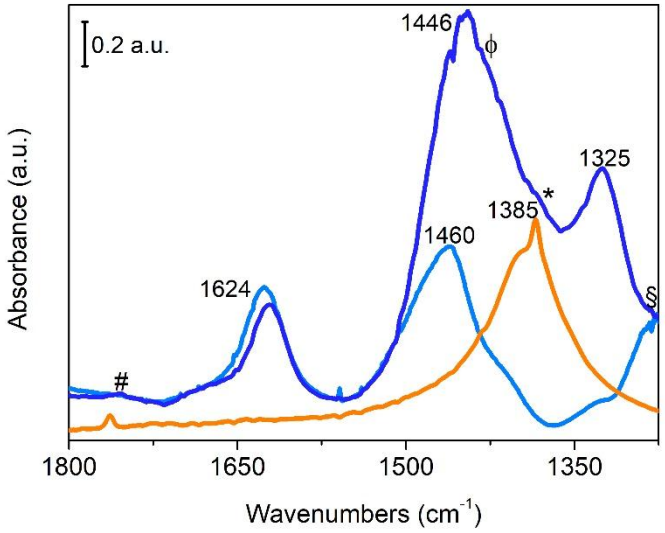

*Figure 3. Comparison between in situ FTIR spectra of Cu-CHA and the spectrum of solid NH_4NO_3. Light blue: NH_3 exposure of the O_2-activated sample; blue: NO/NH_3 exposure after equilibration in NO/O_2; orange: NH_4NO_3. Symbols: #: NO_3^- $\nu_{sym}+\delta_{in\text{-}plane}$ combination mode; *: NO_3^- ν_{asym}; §: Cu-NH_3 out of plane wagging mode; . ϕ: νNO_{2asym} of monodentate Cu-nitrate.*

Features related to ammonium nitrate are observed at 1755 cm^{-1} (combination mode of NO_3^- $\nu_{sym}+\delta_{in\text{-}plane}$) and at 1385 cm^{-1} ($\nu_{asym}NO_3^-$ with a contribution from $\delta_{asym}NH_4^+$), labelled with # and *, respectively in the Cu-CHA spectrum measured upon exposure of the nitrate species to NO/NH_3 (blue curve in Figure 3). Nonetheless, these findings show that despite the formation of a small amount of ammonium nitrate in Cu-CHA under the applied experimental conditions, this species cannot account for the almost doubled intensity of the band at 1446 cm^{-1} (compared to $\delta\,NH_4^+$ at 1460 cm^{-1}), nor for the presence of the peak at 1325 cm^{-1}.

The band at 1325 cm^{-1} is compatible with the presence of covalently linked monodentate nitrates (νNO_{2sym}), which are expected to show the corresponding νNO_{2asym} mode in the 1530-1400 cm^{-1} range.[32, 36] On this basis, we can describe the 1446 cm^{-1} band as a sum of contributions from different chemical species, namely: (i) the bending mode of framework-interacting NH_4^+ ions formed by interaction of NH_3 with the chabazite Brønsted sites (1460 cm^{-1}); (ii) the antisymmetric stretching mode of 'free' NO_3^- (not covalently bonded, with D_{3h} symmetry) from ammonium nitrate (1385 cm^{-1}); (iii) the antisymmetric stretching mode of a monodentate (covalently linked) copper nitrate (*ca.* 1430 cm^{-1}, labelled with ϕ in Figure 3). This explains the shift in frequency and higher intensity with respect to what observed when NH_3 is simply interacting with H^+ ions (light blue curve in Figure 3).

We thus put forward the hypothesis that, under the present conditions, ammonia ligands are displacing the $Z[Cu^{II}(NO_3)]$ complexes from the two framework oxygen ligands (see left-hand structure, Scheme 1) while converting the nitrate ligands from bidentate to monodentate conformation. Thus, beside a minor amount of NH_4NO_3, the main species formed on the copper-exchanged chabazite saturated with nitrates upon exposure to the NO/NH_3 are mobile $[Cu^{II}(NH_3)_3(NO_3)]^+$ complexes. These structures rise from a change in the configuration of the chelating bidentate nitrates previously formed, due to the interaction of NH_3 with copper ions. Ammonia molecules would link to the metal center (giving the 1624 cm^{-1} band), converting the chelating structure to a monodentate one (giving the 1430-1325 cm^{-1} bands). The so-formed entity is mobile, as Cu ions are detached from the zeolite framework.

To further support this hypothesis, and to get information on the oxidation state of the involved ions, *in situ* XAS and UV-Vis-NIR Diffuse Reflectance spectroscopies coupled to DFT calculations have been applied.

In situ XAS

Figure 4 mirrors the FTIR results shown in Figure 1, presenting the evolution of the XAS features upon exposure of Cu-nitrate species in Cu-CHA to a NO/NH_3 feed at 50 °C. In line with FTIR results and previous reports,[4, 10, 17] Cu^{II}-nitrates moieties, $Z[Cu^{II}(NO_3)]$, dominate the initial state of the catalyst (red thick lines in Figure 4). XANES highlights a virtually pure Cu^{II} oxidation state. The fingerprint peak at ca. 3 Å in the phase-uncorrected FT-EXAFS spectrum[4, 17] implies the presence of Cu-nitrates in chelating bidentate configuration. While a second-shell peak is visible, underpinning the presence of framework-coordinated species,[4, 6] its shape is perturbed with respect to what has been previously reported under comparable conditions at higher temperature.[4, 17] Consistently with the FTIR results discussed above, this could be due to the simultaneous presence of a small fraction of framework-coordinated monodentate $Z[Cu^{II}(NO_3)]$ species. Indeed, these species are expected to show scattering contributions from N and O atoms in the second-shell region, where also the Cu-T_{fw} paths contribute (T_{fw} denotes Al/Si atoms in tetrahedral sites of the zeolite framework).

We observe important modifications upon exposure to the NO/NH_3 mixture at 50 °C (grey thin and blue thick lines in Figure 4, for intermediate and final state, respectively). In the XANES, the intensity of the white-line peak at ca. 8997 eV progressively decreases, while evolving towards a characteristic broadened doublet shape. While most of the Cu ions remain in the Cu^{II} oxidation state, a very minor Cu^{I} contribution becomes appreciable (< 10% total Cu) through the development of a rising-edge shoulder at ca. 8982 eV. Noteworthy, at 200 °C under the same gas feed and pre-treatment conditions, the NO/NH_3 mixture has been shown to completely reduce Cu^{II}-nitrates to Cu^{I} species:[4] it is clear that operation temperature strongly influences the reduction kinetics and the Cu^{II}/Cu^{I} ratio in the final state.

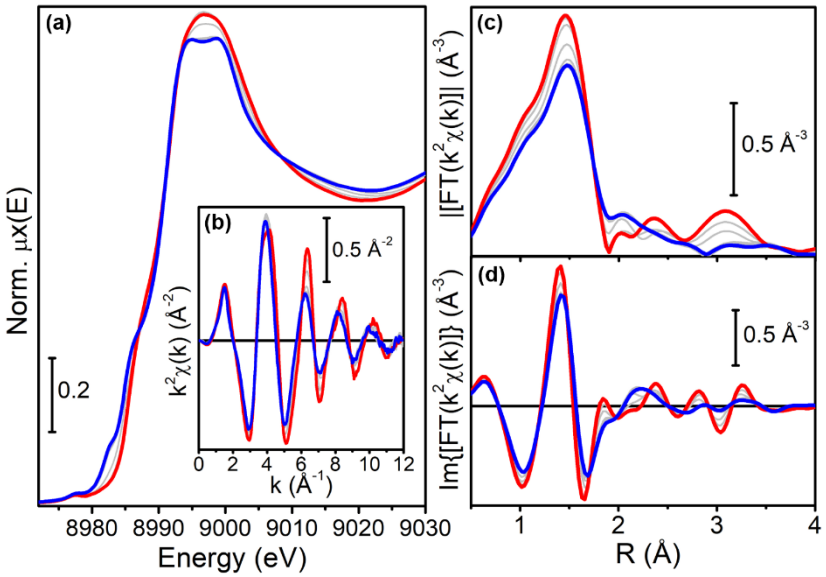

Figure 4. In situ XAS spectra of Cu-CHA during NO/NH_3 interaction (grey thin and blue thick lines: intermediates and final state, respectively) after equilibration in NO/O_2 (red thick curves) (a): Cu K-edge XANES spectra; (b) k^2-weighted $k^2\chi(k)$ EXAFS curves. (c) Magnitude and (d) imaginary part of the Fourier-transformed EXAFS spectra obtained transforming the $k^2\chi(k)$ curves in part (b) in the (2.0-11.8) $Å^{-1}$ range.

Looking at the FT-EXAFS spectra, we notice a gradual shift of the first shell peak to larger distances, accompanied by an intensity decrease. Simultaneously, both the second and the third maxima in the FT-EXAFS are eroded, replaced by an unstructured signal in the final state. These evidences support the efficient NH_3-driven mobilization of the Cu ions[3c, 4, 5c, 6, 9a, 9c, 34] as well as the loss of Cu-nitrate moieties in the chelating bidentate configuration, detected by both XAS and FTIR in the presence of NO/O_2

The XAS results described above are consistent with the formation of NH_3-solvated Cu^{II} species. The *in situ* XAS of Cu-CHA under the NO/NH_3 mixture (Figure 5, blue thick lines) were thus compared with the XAS spectra of the $[Cu(NH_3)_4]^{2+}$ reference compound (Figure 5, green thick lines), measured in aqueous solution.[4] It is thus evident that the Cu-species hosted in Cu-CHA possess strong similarity with the square-planar $[Cu(NH_3)_4]^{2+}$ complexes, but are not the same. Indeed, in line with recent observations of low-temperature NH_3 interaction with Cu-CHA,[9c] the *in situ* XANES for Cu-CHA shows systematically broadened features, in both the rising-edge and white-line region, consistent with the formation of mixed-ligand NH_3-solvated Cu^{II}-species. EXAFS also shows substantial analogies, supporting a first-shell coordination number of ca. four N/O ligands (almost indistinguishable from EXAFS due to their similar backscattering amplitude). Nonetheless, we note a slight intensity decrease of the first-shell peak for Cu-CHA with respect to the $[Cu(NH_3)_4]^{2+}$ reference and certain modifications in the signal structure at higher R-space values.

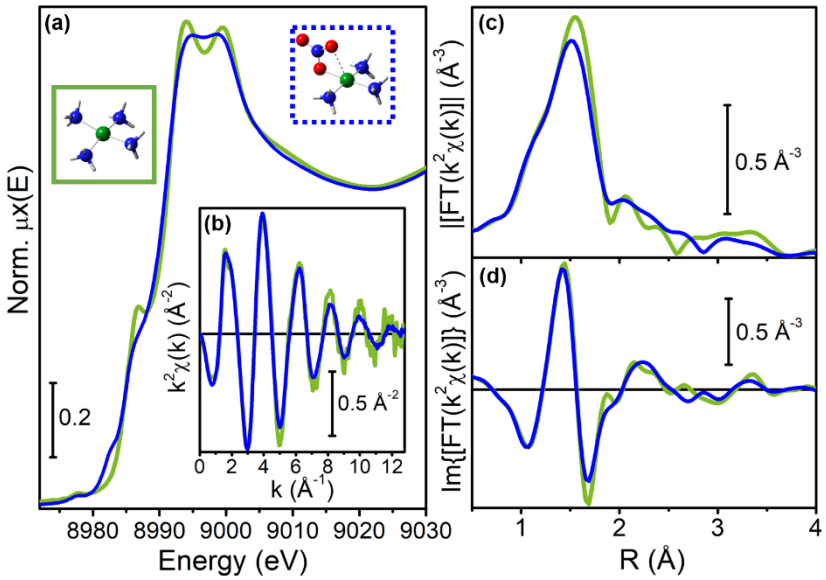

Figure 5. Comparison between in situ static XAS spectra of Cu-CHA after exposure to NO/ NH_3 (blue) and $[Cu(NH_3)_4]^{2+}$ model compound in aqueous solution (green). (a): Cu K-edge XANES spectra; (b) k^2-weighted $k^2\chi(k)$ EXAFS spectra. (c) Magnitude and (d) imaginary part of the Fourier-transformed EXAFS spectra obtained transforming the $k^2\chi(k)$ curves in part (b) in the (2.4-12.4) $Å^{-1}$ range. The insets of part (a) report molecular models of $[Cu(NH_3)_4]^{2+}$ (green solid box) and of the proposed $[Cu^{II}(NH_3)_3(NO_3)]^+$ *complexes (dashed blue box). Cu, green; H, white; O, red; N, blue.*

These observations, taken together with the FTIR results presented above, lead us to propose mobile $[Cu^{II}(NH_3)_3(NO_3)]^+$ complexes to form under exposure of $Z[Cu^{II}(NO_3)]$ moieties to the NO/NH_3 mixture (Figure 5 inset, blue dashed box). Both XAS (erosion of the characteristic peak at ca. 3 Å, stemming from collinear MS contributions characteristic of bidentate chelating nitrates[4, 17]) and FTIR (1430-1325 cm^{-1} bands) support a preferential monodentate-like configuration for these peculiar NH_3-solvated Cu-nitrate species. Driven by these insights, we turned to computational analysis to explore in more detail the coordination mode of nitrate moieties to NH_3-mobilized Cu^{II} centers.

Computational analysis and DFT-assisted EXAFS fitting

Three possible conformers differently arranging the ammonia molecules and nitrate anion around Cu^{II} ions were considered, *i.e.* **A**, **B** and **C** (Scheme 1). The **A** structure is a purely planar complex in which nitrate is monodentate to copper, whereas **C** is a non-planar complex in which nitrate is bidentate (chelated) to copper. Complex **B** is half way between **A** and **C**: here Cu mainly interacts on the plane, but there is still a small bidentate character of the nitrate group. We performed geometry optimization of **A**, **B** and **C** complexes at the B3LYP-D3 level with BS1 and BS2 both in gas phase and in ammonia solution, to simulate the NH_3-rich environment 'felt' by the complex in the zeolite pores under the relevant experimental conditions adopted in this work. The relative stabilities and geometry parameters are reported in Table 2. The differences between BS1 and BS2 results are small from an energetic and geometrical point of view. This validates the use of the smaller BS1 in more complex scenarios, e.g. Cu complexes within the zeolite framework. In gas phase the most stable complex is **C**. Conversely, **B** is more stable when solvated by ammonia. **A** complex is the least stable in both conditions and will not be considered further. Experimentally, the data are gathered in ammonia flow, so we expect the solvation condition to be more representative of the experiments. Including solvation leads to Cu-nitrate species with increased monodentate character, as seen in complex **B**. Indeed, the O-Cu distance (b) is elongated by 0.22 Å with respect to the model without solvation. Thus, the complex **B**, relaxed with the B3LYP-D3/BS2/PCM approach (Scheme 1), has been taken into account for the EXAFS analysis.

Furthermore, the vibrational frequencies of **B** and **C** complexes have been computed considering the solvated cases. The effect of solvation has been evaluated by comparing complex **C** in gas phase. The results are listed in Table 1, considering the three NO_3^- stretching modes (ν_1, ν_2 and ν_3, see Scheme 1 for assignment) and δNH_3. In agreement with experimental results, the computed δNH_3 frequency is hardly affected by the environment (solvent or gas) and by the organization around Cu atom (**B** or **C** structure). Concerning the nitrate modes, the attention is focused on ν_3, which has a character of νN=O for bidentate complexes. In fact, ν_1 and ν_2 cannot be experimentally detected in most cases, since falling in the zeolite 'blind region' (below 1250 cm^{-1}). The computed ν_3 mode for complex **C** in gas phase (no solvent) is in good agreement with the experimental value for $Z[Cu^{II}(NO_3)]$. When solvation of **C** complex is considered, ν_3 is sensibly red-shifted, with concomitant blue-shift of ν_1 and ν_2. This indicates a weakening of the N=O bond (as a consequence of the oxygen atom lone pair interaction with the solvent) and a consequent strengthening of the N-O bonds involved in the coordination of Cu ions (see Scheme 1). This effect is more evident in the case of complex **B**, which can be mainly described as monodentate and is tentatively proposed as model structure responsible for the observed experimental spectra.

Table 1. Comparison between experimental and computed harmonic frequencies in cm^{-1}.

Complex	ν_3NO	ν_1NO	ν_2NO	δNH_3
Computed				
$[Cu^{II}(NH_3)_3(NO_3)]^+$ B solv	1522	1290	1039	1650/1673
$[Cu^{II}(NH_3)_3(NO_3)]^+$ C solv	1567	1242	1049	1665
$[Cu^{II}(NH_3)_3(NO_3)]^+$ C gas	1670	1192	1019	1655/1681
Experimental				
$[Cu^{II}(NH_3)_3(NO_3)]^+$	1430	1325	n.d.	1624
$Z[Cu^{II}(NO_3)]$	1610/1575	n.d.	n.d.	-

n.d.: not detectable

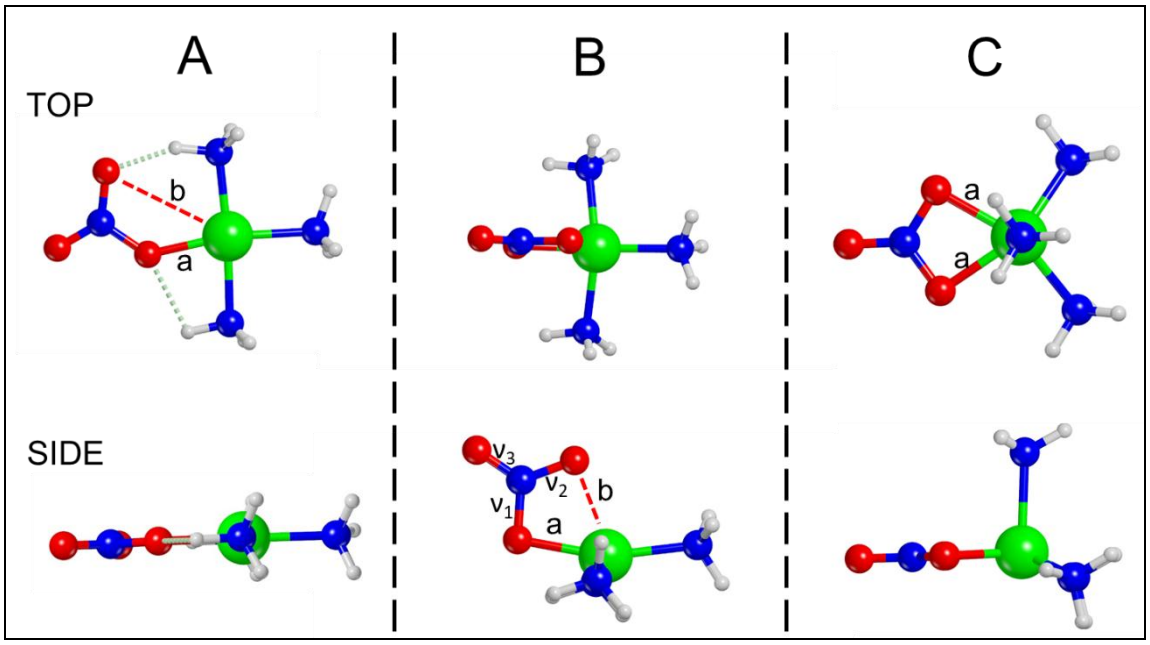

Scheme 1. Top and side view of the computed $[Cu^{II}(NH_3)_3(NO_3)]^+$ *complexes. a and b indicates the Cu-O distances listed in Table 2. Color code: N, blue; O, red; H, gray; Cu, green. In complex* ***A*** *the H-bonds are also reported with dashed light green lines. The assignment of computed* ν_1, ν_2 *and* ν_3 *is shown in complex* ***B****.*

Table 2. Relative stabilities and geometry parameters of the computed $[Cu^{II}(NH_3)_3(NO_3)]^+$ *complexes. Energy in* $kJ{\cdot}mol^{-1}$ *and distances in Å.*

BS:	**A**	**B**	**C**
BS1	a=1.954 b=3.299 ΔE=24.7	a=1.995 b=2.237 ΔE=3.3	a=2.030 ΔE=0.0
BS2	a=1.944 b=3.281 ΔE=27.7	Not stable	a=2.025 ΔE=0.0
BS1 in NH_3	not stable	a=2.046 b=2.458 ΔE=-16.8	a=2.090 ΔE=0.0
BS2 in NH_3	not stable	a=2.036 b=2.455 ΔE=-15.2	a=2.075 ΔE=0.0

In our endeavor to further validate the obtained theoretical models, we employed the $[Cu^{II}(NH_3)_3(NO_3)]^+$ geometry from computational analysis as a starting guess to fit the *in situ* EXAFS obtained for Cu-CHA under exposure to NO/NH_3. We preliminarily benchmarked the method considering the $[Cu^{II}(NH_3)_4]^{2+}$ model compound. EXAFS analysis of the solution-phase spectrum of $[Cu^{II}(NH_3)_4]^{2+}$ using the corresponding DFT-optimized geometry (Figure 6a) resulted in an excellent reproduction of the experimental signal (Figure 6c,d). Table 3 reports an overview of the fitting results: all the guessed parameters are optimized to physically meaningful values. The refined Cu–N1 bond distance of 2.036 ± 0.002 Å is in good agreement with the DFT value of 2.042 Å.

Hence, we moved to the EXAFS analysis of NH_3-solvated Cu-nitrates moieties in Cu-CHA, based on the DFT-optimized $[Cu^{II}(NH_3)_3(NO_3)]^+$ structure **B** (Figure 6b). Overall, the geometry ensured a good reproduction of the experimental EXAFS spectrum of Cu-CHA under NO/NH_3 exposure, with physically realible values of all the optimized parameters (Figure 6e,f and Table 2). The distorted monodentate-like Cu-nitrate species predicted by DFT appears consistent with EXAFS results. Unfortunately, tentative fits performed by independently optimizing the Cu-N1 and Cu-O1 distances were unconclusive, due to excessively high correlations (> 0.9) between the respective radial shift parameters. This is not surprising, due to the EXAFS difficulty in discriminating among O and N atomic neighbours. We thus obtained an average view on the first-shell environment of the Cu centres.

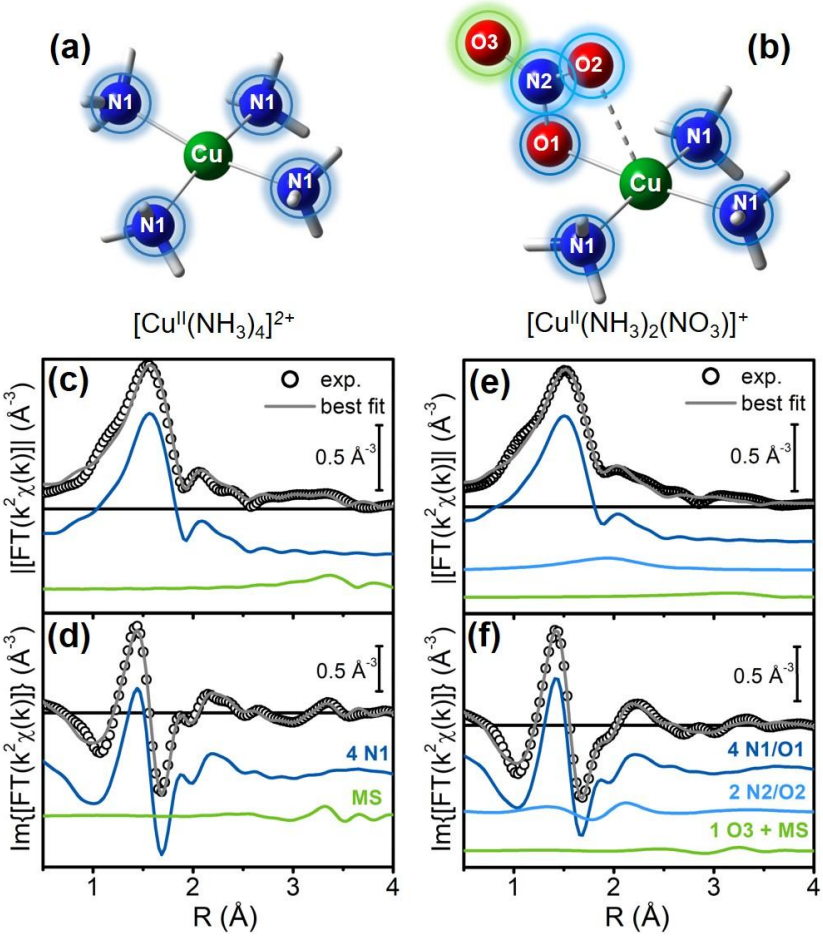

*Figure 6. Cu local environment in DFT-optimized models of (a) $[Cu^{II}(NH_3)_4]^{2+}$ and (b) $[Cu^{II}(NH_3)_3(NO_3)]^+$ species (structure **B** in Scheme 1). The atoms present in the first (N1, O1), second (N2, O2) and third (O3) coordination shell of the Cu absorber are differentiated by blue, light blue and green circles, respectively. Atoms colour code in the models: Cu, green; H, white; O, red; N, blue. (c, d) Comparison between experimental and best fit FT-EXAFS spectra (magnitude and imaginary parts in panels (b) and (c), respectively) using the $[Cu^{II}(NH_3)_4]^{2+}$ geometry in part (a) as initial guess. The principal contributions to the EXAFS signal are also reported, vertically translated for clarity. (e, f) As parts (c, d), but for the spectrum of Cu-CHA under static conditions after exposure to NO/NH_3 using the $[Cu^{II}(NH_3)_3(NO_3)]^+$ geometry in part (b) as starting guess in the fit.*

We observe a larger first-shell DW factor $\sigma^2_{N1/O1}$ with respect to the $[Cu^{II}(NH_3)_4]^{2+}$ reference case, in line with the higher static disorder connected with mixed ligation to the three N1(NH_3) and one O1(NO_3^-) atoms.

Together with modest antiphase effects between the scattering contribution of N1/O1 and N2/O2 atoms (Figure 6e,f), this explains the lower intensity of the first-shell peak in the EXAFS of Cu-CHA with respect to the $[Cu^{II}(NH_3)_4]^{2+}$ reference, although we are dealing in both cases with four-fold coordinated Cu-complexes.

Data analysis also revealed a slight elongation of the average first-shell Cu-N1/O1 bond distance with respect to the DFT value, whereas the subsequent coordination shells are optimized at slightly larger distances. Considering the model in Figure 6b, it is clear that we are dealing with a rather flexible nitrate coordination mode. Also in the view of the finite data collection temperature in the XAS experiments, we can envisage a more 'bent' nitrate coordination with respect to the one predicted by DFT, resulting in unaltered Cu–O1 distance but increased bond lengths for the O2, N2 and O3 atomic neighbours.

Table 3. Best-fit parameters optimized in the DFT-assisted EXAFS fit of the k^2-weighted EXAFS spectra of the $[Cu^{II}(NH_3)_4]^{2+}$ model compound and of Cu-CHA under static conditions after exposure to NO/ NH_3 at 50 °C. Selected DFT-optimized bond distances are reported for comparison.

Fit parameters	**$[Cu^{II}(NH_3)_4]^{2+}$ (solution)**		**$[Cu^{II}(NH_3)_3(NO_3)]^{+}$ (Cu-CHA)**	
	DFT	*EXAFS*	*DFT*	*EXAFS*
S_0^2		0.90 ± 0.06		0.90[a]
ΔE (eV)		1.7 ± 0.5		− 1.7 ± 0.7
Fit R-factor		0.00933		0.01050
n° par. (n° ind.)		4 (19)		5 (19)
$<R_{N1/O1)}>$ (Å)	2.042	2.036 ± 0.002	2.035	2.00 ± 0.01
$\sigma^2_{N1/O1}$ (Å^2)		0.0049 ± 0.0005		0.0067 ± 0.0004
R_{O2} (Å)	–	–	2.455	2.55 ± 0.02[b]
σ^2_{O2} (Å^2)	–	–	–	0.010 ± 0.003[c]
R_{N2} (Å)	–	–	2.640	2.75 ± 0.02[b]
$\sigma^2_{O2/N2}$ (Å^2)	–	–	–	0.010 ± 0.003[c]
R_{O3} (Å)	–	–	3.839	3.99 ± 0.04[b]
σ^2_{O3} (Å^2)	–	–	–	0.012 ± 0.004[c]

[a] Fixed to the best-fit value obtained for the $[Cu^{II}(NH_3)_4]^{2+}$ reference to avoid excessively high correlations with σ^2 parameters
[b] Calculated from the best-fit value of α_{far} = (0.09 ± 0.02) Å for direct comparison with DFT-optimized geometry.
[c] Calculated from the best-fit value of σ^2_{far} = (0.010 ± 0.003) Å^2.

In situ Diffuse Reflectance UV-Vis-NIR spectroscopy

UV-Vis-NIR Diffuse Reflectance spectroscopy was also used to monitor the reactivity of framework-interacting $Z[Cu^{II}(NO_3)]$ moieties with the NO/NH_3 mixture, by following the changes in the Cu local structure by means of ligand-field $d-d$ and Ligand to Metal Charge-Transfer (LMCT) transitions. Figure 7 reports the evolution of the spectra measured at 50 °C upon exposure of the pre-formed copper nitrates to NO/NH_3, compared to the spectra obtained during direct exposure of the fresh O_2-activated catalyst to NH_3 (right-hand panel). The spectra are reported in reflectance (R%), to avoid artefacts associated with data treatment when applying the Kubelka-Munk function or the Pseudo-Absorbance conversion.[37]

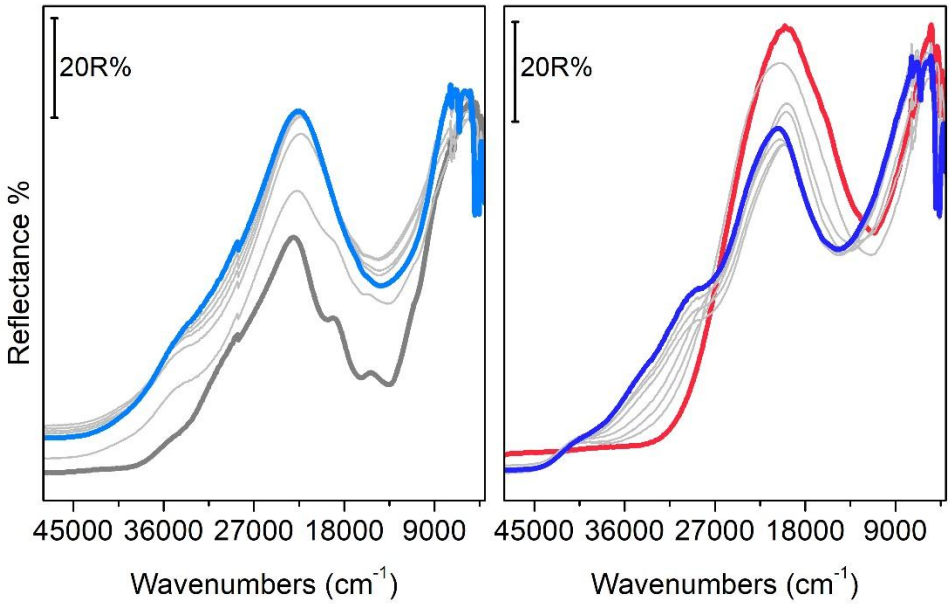

Figure 7. In situ UV-Vis-NIR diffuse reflectance spectra of Cu-CHA during: exposure of fresh O_2 activated catalyst to NH_3 (left) and exposure to NO/NH_3 after equilibration in NO/O_2 flow (right). Left) grey thick line: catalyst pre-activated in O_2 at 400°C; light blue thick line: finale state in NH_3. Right) red thick line: after equilibration in NO/O_2; blue thick line: final state in NO/NH_3. Grey thin lines: intermediates spectra over 60 min.

As previously observed by FTIR (Figure 2), the final states obtained at the end of the two experiments are different (compare light blue and blue curves), further confirming that we are dealing with different Cu local structures.

The data shown in the left-hand panel of Figure 7 (reported for comparison) are obtained exposing the fresh O_2-activated catalyst (grey curve) to NH_3 (light blue curve). The starting point is the typical spectrum of O_2-activated Cu-CHA[38] and can be explained with the presence a variety of Cu-oxo/hydroxo monomeric and dimeric cores.[38e, 39] The spectrum obtained after NH_3 exposure is characterized by a broad $d-d$ transition centered at 14100 cm^{-1} and by a CT transition at 31500 cm^{-1} (measured at half height). These features are comparable to those recently published by Borfecchia *et al*. (obtained on the same O_2-activated catalyst exposed to NH_3 at 200 °C)[9c] meaning that we are dealing with the same chemical species, namely, a mobile $[Cu^{II}(NH_3)_3(OH^-)]^+$ complex. The spectrum of the 'pure' $[Cu^{II}(NH_3)_4]^{2+}$ complex in aqueous solution (green curve in Figure 8) differs from that obtained in the zeolite both for the position of the $d-d$ maximum (shifted from around 17000 to 14100 cm^{-1}) and for the presence of a well-defined band around 32000 cm^{-1} in the CT tail. As discussed elsewhere,[9c] these differences can be explained considering the presence of the OH^- extra ligand in the $[Cu^{II}(NH_3)_3(OH)]^+$ complex, which affects the coordination sphere of Cu^{II} ions both in the splitting of $d-d$ orbitals[40] and in the position and shape of the LMCT profile. More in detail, the blue-shift of the LMCT profile can be associated with the detachment of Cu^{II} ions from the chabazite framework by NH_3 ligands. This is in agreement with the higher optical electronegativity of the N_{NH3} atoms with respect to the O_{fw} ones.[41]
The evolution of the spectra obtained exposing the Cu-CHA sample saturated with nitrates to NO/NH_3 are reported in the right-hand panel of Figure 7. The final state of the catalyst after NO/O_2 exposure at 50 °C (red curve) is characterized by an intense ligand-to-metal CT transition at 26000 cm^{-1} (measured at half height) and by a symmetrical and well-defined $d-d$ transition, centered at 11000 cm^{-1}. These features are in agreement with those reported in literature for bidentate nitrate species, both in Cu-CHA [17] and in homogeneous Cu^{II} complexes.[42] Indeed, the low energy $d-d$ transitions can be related to the highly-

symmetrical local geometry of Cu ions when forming chelating Z[$Cu^{II}(NO_3)$] species, while the CT position, ascribed to the $O_{NO_3^-} \rightarrow Cu^{2+}$ LMCT, is in agreement with the formation of a complex with a high degree of O-Cu bond covalence. Notice that this technique cannot discriminate the presence of a small fraction of monodentate nitrate complexes (observed by FTIR) due to the broadness of the bands.

When the Z[$Cu^{II}(NO_3)$] phase is exposed to the NO/NH_3 gas feed, the spectra show significant changes. First, we observe the growth of peaks associated with NH_3/NH_4^+, adsorbed on Cu ions and on zeolite Brønsted sites, in the NIR region. Secondly, changes associated with the modification of the ligand sphere surrounding Cu ions are observed in the $d-d$ and LMCT regions. In fact, the $d-d$ maximum becomes more asymmetric and shifts to higher energy (14700 cm^{-1}). The LMCT profile shows an overall blue-shift and a progressive development of an intense shoulder at 27500 cm^{-1}, together with the growth of two weaker features at 32000 and 38000 cm^{-1}.
The blue-shift of $d-d$ and LMCT transitions is in agreement with the formation of the mixed ligand $[Cu^{II}(NH_3)_3(NO_3)]^+$ complex proposed above. The assignment of the three features in the Charge Transfer low energy tail is not straightforward. On the basis of the considerations on optical electronegativity previously done, we can hypothesize that the first shoulder (centered at 27500 cm^{-1}) is associated with the $O_{NO_3^-} \rightarrow Cu^{2+}$ LMCT, while those at 32000 and 38000 cm^{-1} are due to $N_{NH_3} \rightarrow Cu^{2+}$ transitions. Further support to this assignment can be found in the data reported in Figure 8, where the spectrum of $[Cu^{II}(NH_3)_4]^{2+}$, $[Cu^{II}(NH_3)_3(OH)]^+$ (that is, the final state after exposure of the O_2-activated sample to NH_3) and that assigned to $[Cu^{II}(NH_3)_3(NO_3)]^+$ complexes are directly compared. Indeed, the feature at 27500 cm^{-1} is not present in the spectrum of nitrates copper complexes (red curve in Figure 7),[17] nor in the ammonia copper complexes $[Cu^{II}(NH_3)_4]^{2+}$ and $[Cu^{II}(NH_3)_3(OH)]^+$. Thus, we can propose that the intense absorption at 27500 cm^{-1} is a fingerprint of the mixed ligand $[Cu^{II}(NH_3)_3(NO_3)]^+$ complex, in agreement with the fact that the specific intensity of a charge transfer transition is influenced by the overlap between the involved metal and ligands orbitals.[42]

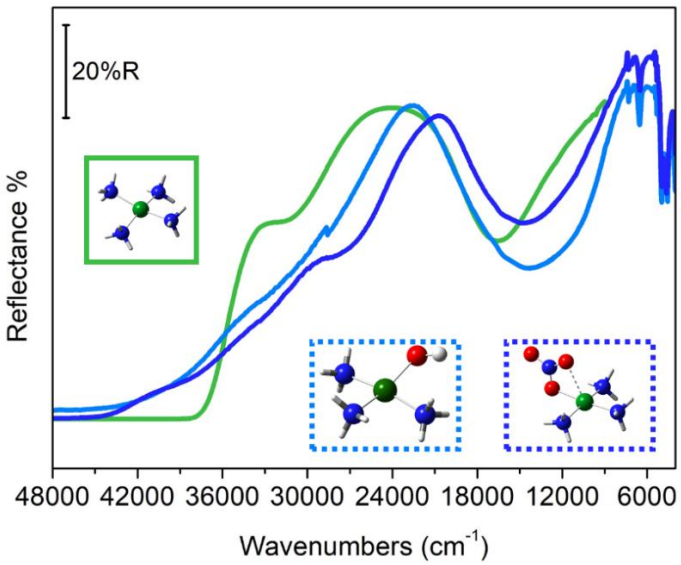

Figure 8. Comparison of in situ UV-Vis-NIR DR spectra of $[Cu^{II}(NH_3)_3(OH)]^+$ formed by dosing NH_3 on O_2-activated Cu-CHA (light blue), $[Cu^{II}(NH_3)_3(NO_3)]^+$ formed by dosing NO/NH_3 after equilibration in NO/O_2 (blue) and $[Cu^{II}(NH_3)_4]^{2+}$ model compound in aqueous solution (green). The schematic representation of the mentioned complexes is reported for sake of clarity. Atoms colour code in the models: Cu, green; H, white; O, red; N, blue.

Conclusions

In the present work, the formation of a mobile $[Cu^{II}(NH_3)_3(NO_3)]^+$ complex is proposed for the first time as a result of NO/NH_3 (or NH_3 alone) interaction with framework-interacting Cu-nitrates at 50 °C in the Cu-CHA

catalyst. The proposed structure is based on results from different spectroscopic techniques, in parallel with DFT calculations to evaluate the stability of the complex.

In situ FTIR spectroscopy was used as a primary technique to identify the formed mixed-ligand Cu complexes. The obtained results allowed us to discriminate the spectroscopic contribution of Cu ligands among those of the species adsorbed on chabazite surface (including NH_4^+ and a small fraction of NH_4NO_3) and to partially re-discuss band assignment. We have thus identified the bands of the monodentate nitrate group linked to Cu ions, while confirming their strong interaction with NH_3 molecules.

At variance with what is observed under similar conditions at 200 °C, XAS and UV-Vis-NIR diffuse reflectance spectroscopies showed a negligible Cu^{II} to Cu^{I} reduction at this temperature. The change in the coordination sphere of the Cu^{II} ions detached by NH_3 from framework oxygen atoms, was nicely followed by both techniques. In particular, diffuse reflectance UV-Vis-NIR showed the appearance of peculiar bands at 27500 cm^{-1} (with minor components at 32000 and 38000 cm^{-1}) which are ascribed to the mixed-ligand coordination sphere. The reliability of the proposed $[Cu^{II}(NH_3)_3(NO_3)]^+$ structure was confirmed by DFT calculations, showing that the nitrate monodentate configuration is favored by NH_3 solvation. The optimized geometry was successfully used for EXAFS fitting of the corresponding experimental data. The proposed structure could be considered by researchers working in the field while investigating the low temperature SCR mechanism.

Acknowledgments

M. Cutini would like to express his gratitude to his mentor, Prof. Piero Ugliengo, for his permission to carry out research and build-up collaborations, independently and with freedom.

Keywords

Cu-CHA; FTIR spectroscopy; UV–Vis spectroscopy; nitrates; SCR

References

[1] A. M. Beale, F. Gao, I. Lezcano-Gonzalez, C. H. F. Peden, J. Szanyi, *Chem. Soc. Rev.* **2015**, *44*, 7371-7405.

[2] E. Borfecchia, P. Beato, S. Svelle, U. Olsbye, C. Lamberti, S. Bordiga, *Chem. Soc. Rev.* **2018**, *47*, 8097-8133.

[3] a) E. Borfecchia, K. A. Lomachenko, F. Giordanino, H. Falsig, P. Beato, A. V. Soldatov, S. Bordiga, C. Lamberti, *Chem. Sci.* **2015**, *6*, 548-563; b) A. Martini, E. Borfecchia, K. A. Lomachenko, I. A. Pankin, C. Negri, G. Berlier, P. Beato, H. Falsig, S. Bordiga, C. Lamberti, *Chem. Sci.* **2017**, *8*, 6836-6851; c) C. Paolucci, A. A. Parekh, I. Khurana, J. R. Di Iorio, H. Li, J. D. Albarracin Caballero, A. J. Shih, T. Anggara, W. N. Delgass, J. T. Miller, F. H. Ribeiro, R. Gounder, W. F. Schneider, *J. Am. Chem. Soc.* **2016**, *138*, 6028-6048; d) J. R. Di Iorio, R. Gounder, *Chem. Mat.* **2016**, *28*, 2236-2247.

[4] T. V. W. Janssens, H. Falsig, L. F. Lundegaard, P. N. R. Vennestrøm, S. B. Rasmussen, P. G. Moses, F. Giordanino, E. Borfecchia, K. A. Lomachenko, C. Lamberti, S. Bordiga, A. Godiksen, S. Mossin, P. Beato, *ACS Catal.* **2015**, *5*, 2832-2845.

[5] a) L. Chen, H. Falsig, T. V. W. Janssens, H. Gronbeck, *J. Catal.* **2018**, *358*, 179-186; b) L. Chen, H. Falsig, T. V. W. Janssens, J. Jansson, M. Skoglundh, H. Gronbeck, *Catal. Sci. Technol.* **2018**, *8*, 2131-2136; c) C. Paolucci, I. Khurana, A. A. Parekh, S. C. Li, A. J. Shih, H. Li, J. R. Di Iorio, J. D. Albarracin-Caballero, A. Yezerets, J. T. Miller, W. N. Delgass, F. H. Ribeiro, W. F. Schneider, R. Gounder, *Science* **2017**, *357*, 898-903.

[6] K. A. Lomachenko, E. Borfecchia, C. Negri, G. Berlier, C. Lamberti, P. Beato, H. Falsig, S. Bordiga, *J. Am. Chem. Soc.* **2016**, *138*, 12025-12028.

[7] F. Gao, D. Mei, Y. Wang, J. Szanyi, C. H. F. Peden, *J. Am. Chem. Soc.* **2017**, *139*, 4935–4942.

[8] A. Marberger, A. W. Petrov, P. Steiger, M. Elsener, O. Krocher, M. Nachtegaal, D. Ferri, *Nat. Catal.* **2018**, *1*, 221-227.

[9] a) F. Giordanino, E. Borfecchia, K. A. Lomachenko, A. Lazzarini, G. Agostini, E. Gallo, A. V. Soldatov, P. Beato, S. Bordiga, C. Lamberti, *J. Phys. Chem. Lett.* **2014**, *5*, 1552-1559; b) A. G. Greenaway, I. Lezcano-Gonzalez, M. Agote-Aran, E. K. Gibson, Y. Odarchenko, A. M. Beale, *Top. Catal.* **2018**, *61*, 175-182; c) E. Borfecchia, C. Negri, K. A. Lomachenko, C. Lamberti, T. V. W. Janssens, G. Berlier, *React. Chem. Eng.* **2019**, in press, doi: 10.1039/C1038RE00322J; d) L. Chen, T. V. W. Janssens, M. Skoglundh, H. Grönbeck, *Top. Catal.* **2018**, in press, DOI: 10.1007/s11244-11018-11095-y.

[10] C. Negri, P. S. Hammershoi, T. V. W. Janssens, P. Beato, G. Berlier, S. Bordiga, *Chem.–Eur. J* **2018**, *24*, 12044-12053.

[11] a) M. Colombo, I. Nova, E. Tronconi, *Catal. Today* **2012**, *197*, 243-255; b) M. P. Ruggeri, J. Y. Luo, I. Nova, E. Tronconi, K. Kamasamudram, A. Yezerets, *Catal. Today* **2018**, *307*, 48-54; c) M. P. Ruggeri, I. Nova, E. Tronconi, J. A. Pihl, T. J. Toops, W. P. Partridge, *Appl. Catal. B-Environ.* **2015**, *166*, 181-192.

[12] a) I. Nova, C. Ciardelli, E. Tronconi, D. Chatterjee, B. Bandl-Konrad, *Catal. Today* **2006**, *114*, 3-12; b) A. Savara, M. J. Li, W. M. H. Sachtler, E. Weitz, *Appl. Catal. B-Environ.* **2008**, *81*, 251-257.

[13] a) C. Ciardelli, I. Nova, E. Tronconi, D. Chatterjee, B. Bandl-Konrad, *Chem. Commun.* **2004**, 2718-2719; b) L. Cao, L. Chen, X. D. Wu, R. Ran, T. F. Xu, Z. Chen, D. Weng, *Appl. Catal. A-Gen.* **2018**, *557*, 46-54; c) H. Y. Chen, Z. H. Wei, M. Kollar, F. Gao, Y. L. Wang, J. Szanyi, C. H. F. Peden, *J. Catal.* **2015**, *329*, 490-498; d) M. Kantcheva, V. Bushev, D. Klissurski, *J. Catal.* **1994**, *145*, 96-106.

[14] Y. H. Yeom, J. Henao, M. J. Li, W. M. H. Sachtler, E. Weitz, *J. Catal.* **2005**, *231*, 181-193.

[15] Z. Chen, Z. C. Si, L. Cao, X. D. Wu, R. Ranb, D. Weng, *Catal. Sci. Technol.* **2017**, *7*, 2531-2541.

[16] M. Bendrich, A. Scheuer, R. E. Hayes, M. Votsmeier, *Appl. Catal. B-Environ.* **2018**, *222*, 76-87.

[17] C. Tyrsted, E. Borfecchia, G. Berlier, K. A. Lomachenko, C. Lamberti, S. Bordiga, P. N. R. Vennestrom, T. V. W. Janssens, H. Falsig, P. Beato, A. Puig-Molina, *Catal. Sci. Technol.* **2016**, *6*, 8314-8324.

[18] O. Mathon, A. Beteva, J. Borrel, D. Bugnazet, S. Gatla, R. Hino, I. Kantor, T. Mairs, M. Munoz, S. Pasternak, F. Perrin, S. Pascarelli, *J. Synchrotron Radiat.* **2015**, *22*, 1548-1554.

[19] D. Bellet, B. Gorges, A. Dallery, P. Bernard, E. Pereiro, J. Baruchel, *J. Appl. Crystallogr.* **2003**, *36*, 366-367.

[20] S. Bordiga, E. Groppo, G. Agostini, J. A. van Bokhoven, C. Lamberti, *Chem. Rev.* **2013**, *113*, 1736-1850.
[21] B. Ravel, M. Newville, *J. Synchrotron Radiat.* **2005**, *12*, 537-541.
[22] S. I. Zabinsky, J. J. Rehr, A. Ankudinov, R. C. Albers, M. J. Eller, *Phys. Rev. B* **1995**, *52*, 2995-3009.
[23] M. J. Frisch, G. W. Trucks, H. B. Schlegel, G. E. Scuseria, M. A. Robb, J. R. Cheeseman, G. Scalmani, V. Barone, B. Mennucci, G. A. Petersson, *et al*., *Gaussian 09, Revision D.01.* **2013**, *Gaussian, Inc. Wallingford, CT*.
[24] J. P. Perdew, K. Burke, M. Ernzerhof, *Phys. Rev. Lett.* **1996**, *77*, 3865-3868.
[25] S. Grimme, J. Antony, S. Ehrlich, H. Krieg, *J. Chem. Phys.* **2010**, *132*.
[26] A. Schafer, H. Horn, R. Ahlrichs, *J. Chem. Phys.* **1992**, *97*, 2571-2577.
[27] A. Schafer, C. Huber, R. Ahlrichs, *J. Chem. Phys.* **1994**, *100*, 5829-5835.
[28] R. Dovesi, V. R. Saunders, C. Roetti, R. Orlando, C. M. Zicovich-Wilson, F. Pascale, B. Civalleri, K. Doll, N. M. Harrison, I. J. Bush, P. D'Arco, M. Llunell, M. Causà, Y. Noël, L. Maschio, A. Erba, M. Rerat, S. Casassa, **2017**, CRYSTAL17 User's Manual (Università di Torino: Torino, Italy).
[29] F. Weigend, *Phys. Chem. Chem. Phys.* **2006**, *8*, 1057-1065.
[30] S. Miertus, E. Scrocco, J. Tomasi, *Chem. Phys.* **1981**, *55*, 117-129.
[31] G. D. Billaud, A., *J. Phys. Chem.* **1975**, *79*, 3053-3055.
[32] K. I. Hadjiivanov, *Catal. Rev.* **2000**, *42*, 71-144.
[33] A. Zecchina, L. Marchese, S. Bordiga, C. Paze, E. Gianotti, *J. Phys. Chem. B* **1997**, *101*, 10128-10135.
[34] I. Lezcano-Gonzalez, U. Deka, B. Arstad, A. Van Yperen-De Deyne, K. Hemelsoet, M. Waroquier, V. Van Speybroeck, B. M. Weckhuysen, A. M. Beale, *Phys. Chem. Chem. Phys.* **2014**, *16*, 1639-1650.
[35] a) A. Théorêt, C. Sandorfy, *Can. J. Chem.* **1963**, *42*, 57-62; b) J. R. Fernandes, S. Ganguly, C. N. R. Rao, *Spectrochim. Acta* **1979**, *35A*, 1013-1020.
[36] a) D. V. Pozdnyakov, V. N. Filimonov, *Adv. Mol. Relax. Processes* **1973**, *5*, 55-63; b) B. O. Field, C. J. Hardy, *J. Chem. Soc.* **1963**, 4428-4434.
[37] a) F. C. Jentoft, *Adv. Catal.* **2009**, *52*, 129-211; b) F. C. Meunier, *React. Chem. Eng.* **2016**, *1*, 134-141; c) J. Sirita, S. Phanichphant, F. C. Meunier, *Anal. Chem.* **2007**, *79*, 3912-3918.
[38] a) F. Giordanino, P. N. R. Vennestrom, L. F. Lundegaard, F. N. Stappen, S. Mossin, P. Beato, S. Bordiga, C. Lamberti, *Dalton T.* **2013**, *42*, 12741-12761; b) A. Godiksen, F. N. Stappen, P. N. R. Vennestrom, F. Giordanino, S. B. Rasmussen, L. F. Lundegaard, S. Mossin, *J. Phys. Chem. C* **2014**, *118*, 23126-23138; c) B. Ipek, M. J. Wulfers, H. Kim, F. Goltl, I. Hermans, J. P. Smith, K. S. Booksh, C. M. Brown, R. F. Lobo, *ACS Catal.* **2017**, *7*, 4291-4303; d) M. J. Wulfers, S. Teketel, B. Ipek, R. F. Lobo, *Chem. Commun.* **2015**, *51*, 4447-4450; e) C. Negri, M. Signorile, N. Porcaro, E. Borfecchia, G. Berlier, T. V. W. Janssens, S. Bordiga, *Appl. Catal. A-Gen.* **2019**, *in press, DOI: 10.1016/j.apcata.2019.03.018*.
[39] H. Li, C. Paolucci, I. Khurana, L. Wilcox, F. Goltl, J. D. Albarracin-Caballero, A. J. Shih, F. H. Ribeiro, R. Gounder, W. F. Schneider, *Chem. Sci.* **2019**, *10*, 2373-2384.
[40] L. N. Trevani, J. C. Roberts, P. R. Tremaine, *J. Solut. Chem.* **2001**, *30*, 585-622.
[41] a) J. A. Duffy, *J. Chem. Soc., Dalton Trans.* **1983**, 1475-1478; b) A. B. P. Lever, *Inorganic Electronic Spectroscopy (II ed)*, Elsevier, Amsterdam, **1984**.
[42] N. Lehnert, U. Cornelissen, F. Neese, T. Ono, Y. Noguchi, K. Okamoto, K. Fujisawa, *Inorg. Chem.* **2007**, *46*, 3916-3933.